European Journal of Radiology Open 9 (2022) 100442

Contents lists available at ScienceDirect

European Journal of Radiology Open

journal homepage: www.elsevier.com/locate/ejro

Semiautomatic assessment of respiratory dynamics using cine MRI in chronic obstructive pulmonary disease

Hirotaka Sato [a,b], Naoko Kawata [a,*], Ayako Shimada [c], Yuma Iwao [d], Chen Ye [d], Yoshitada Masuda [e], Hideaki Haneishi [d], Koichiro Tatsumi [a], Takuji Suzuki [a]

[a] Department of Respirology, Graduate School of Medicine, Chiba University, 1-8-1, Inohana, Chuo-ku, Chiba-shi, Chiba 260-8677, Japan
[b] Department of Radiology, Soka Municipal Hospital, 2-21-1, Souka, Souka-shi, Saitama 340-8560, Japan
[c] Department of Respirology, Shin-yurigaoka General Hospital, 255 Tsuko, Furusawa, Asao, Kawasaki, Kanagawa 215-0026, Japan
[d] Center for Frontier Medical Engineering, Chiba University, 1-33, Yayoi-cho, Inage-ku, Chiba 263-8522, Japan
[e] Department of Radiology, Chiba University Hospital, 1-8-1, Inohana, Chuo-ku, Chiba-shi, Chiba 260-8677, Japan

ARTICLE INFO

Keywords:
Chronic obstructive pulmonary disease (COPD)
Magnetic resonance imaging (MRI)
Lung area
Diaphragm
Asynchronous movement
Pulmonary function

ABSTRACT

Purpose: The quantitative assessment of impaired lung motions and their association with the clinical characteristics of COPD patients is challenging. The aim of this study was to measure respiratory kinetics, including asynchronous movements, and to analyze the relationship between lung area and other clinical parameters.
Materials and methods: This study enrolled 10 normal control participants and 21 COPD patients who underwent dynamic MRI and pulmonary function testing (PFT). The imaging program was implemented using MATLAB®. Each lung area was detected semi-automatically on a coronal image (imaging level at the aortic valve) from the inspiratory phase to the expiratory phase. The Dice index of the manual measurements was calculated, with the relationship between lung area ratio and other clinical parameters, including PFTs then evaluated. The asynchronous movements of the diaphragm were also evaluated using a sagittal image.
Results: The Dice index for the lung region using the manual and semi-automatic extraction methods was high (Dice index = 0.97 ± 0.03). A significant correlation was observed between the time corrected lung area ratio and percentage of forced expiratory volume in 1 s (FEV_1%pred) and residual volume percentage (RV%pred) ($r = -0.54$, $p = 0.01$, $r = 0.50$, $p = 0.03$, respectively). The correlation coefficient between each point of the diaphragm in the group with visible see-saw like movements was significantly lower than that in the group without see-saw like movements (value = −0.36 vs 0.95, p = 0.001).
Conclusion: Semi-automated extraction of lung area from Cine MRI might be useful for detecting impaired respiratory kinetics in patients with COPD.

1. Introduction

Chronic obstructive pulmonary disease (COPD) is characterized by persistent and progressive airflow obstruction and an abnormal inflammatory response to toxic particles and gases, mainly from smoking [1]. COPD is expected to become the third-leading cause of death

Abbreviations: BMI, body mass index; CAT, chronic obstructive pulmonary disease assessment test; COPD, chronic obstructive pulmonary disease; DL_{CO}, carbon monoxide diffusing capacity of the lung; FEV_1, forced expiratory volume in 1 s; FEV_1/FVC, forced expiratory volume in 1 s per forced vital capacity; FLASH, fast low angle shot; FOV, field of view; FRC, functional residual capacity; FVC, forced vital capacity; GOLD, Global Initiative for Chronic Pulmonary Obstructive Lung Disease; HASTE, Half Fourier Acquisition Single-shot Turbo spin Echo; ICC, intraclass correlation coefficient; ICS, inhaled corticosteroid; LAA, low attenuation area; LABA, long-acting β-2 agonist; LAMA, long-acting muscarinic antagonists; LAV, low attenuation volume; LV, lung volume; MDCT, multi-detector row computed tomography; MRI, magnetic resonance imaging; PFT, pulmonary function testing; RV, residual volume; RV/TLC, residual volume per total lung capacity; SSFP, steady-state free precession; TLA, total lung area; TLC, total lung capacity; UTE, ultrashort echo time.

* Corresponding author.
E-mail addresses: h.sato1980@gmail.com (H. Sato), chumito_03@yahoo.co.jp (N. Kawata), romanholiday52@yahoo.co.jp (A. Shimada), yuma1360@gmail.com (Y. Iwao), yechen@chiba-u.jp (C. Ye), masuda.yoshitada@hospital.chiba-u.jp (Y. Masuda), haneishi@faculty.chiba-u.jp (H. Haneishi), tatsumi@faculty.chiba-u.jp (K. Tatsumi), suzutaku@chiba-u.jp (T. Suzuki).

https://doi.org/10.1016/j.ejro.2022.100442
Received 4 June 2022; Received in revised form 19 September 2022; Accepted 26 September 2022

globally by 2030 and there is a serious concern about the economic healthcare burden associated with the disease [2,3].

Currently, the diagnosis and severity of COPD are assessed physiologically using pulmonary function tests. Recent advances in imaging equipment such as computed tomography (CT) and image analysis methods have revealed morphological features of COPD that could not be captured by respiratory function tests [4–7]. However, static image analysis during breath-hold using chest x-rays or chest CT has been the method mainly investigated. The main focus of these earlier studies was on the relationship between the imaging indices obtained from static images and disease severity and phenotypes [8–10]. Heterogeneity is present in respiration between the left and right lungs and the diaphragm (i.e., loss of simultaneity and asynchronous movements) in patients with COPD. As the disease progresses, it causes hyperinflation of the lungs and deformation of the airways and thorax, thereby contributing to a decreased thoracic motion with respiratory muscle weakness and malnutrition [11,12]. There are only a small number of studies that have evaluated dynamic respiratory abnormalities, with reports on chest dynamics using chest dynamics X-rays [13] and chest 4D-CT [14]. However, due to technical problems and to avoid ionizing radiation, analyses of the diaphragm and the lungs have been limited, and it remains difficult to evaluate the entire lung continuously.

On the other hand, magnetic resonance imaging (MRI) can evaluate structural and functional abnormalities of the lung noninvasively [15]. It has recently become a practical tool in clinical practice. A few previous studies have used MRI to continuously extract respiratory dynamics to examine the relationships between physiological parameters and disease characteristics [16]. In a recent study, we analyzed lung dynamics using cine MRI in order to clarify the relationship of MRI measurements with limited airflow and air trapping in patients with severe COPD [17]. However, the manual methods used were time-consuming and challenging for evaluating continuous lung movements. Several methods for extracting lung fields in MRI scans have been reported, ranging from fully-automated to semi-automated methods [18–20]. For example, semi-automatic segmentation of lungs and tumors [19] and semi-automated process to measure lung volumes have been described [20]. In addition, MRI has a variety of sequences [21], including Steady-state Free Precession (SSFP) [22], fast low angle shot (FLASH) [23], Half Fourier Acquisition Single-shot Turbo spin Echo (HASTE) [24,25], and a time-resolved T1-weighted 3D keyhole pulse sequence [26]. An extraction algorithm tailored to each sequence is required for analysis.

The aim of the current prospective study was to investigate the respiratory dynamics of COPD patients using a combination of cine MRI using the SSFP method and several analysis algorithms of a programming platform. We also used the same extraction algorithms to analyze the asynchronous motions of the diaphragm using sagittal images.

2. Methods

2.1. Participants

The study enrolled 21 patients diagnosed with COPD who underwent chest dynamic MRI at our hospital between April 2011 and September 2019. Most of the participants in the present study had been investigated in a previous study that had a different research objective [17]. All the patients had a history of smoking. COPD was diagnosed according to the criteria of the Global Initiative for Chronic Obstructive Lung Disease (GOLD) [3]. The patients underwent a COPD assessment test (CAT) [27], pulmonary function testing (PFT), and multi-detector row computed tomography (MDCT) imaging within 4 months of undergoing an MRI. Patients were excluded if they had abnormal lung parenchymal lesions other than emphysematous change or heart failure. The normal control participants consisted of 10 healthy volunteers who underwent a PFT and MRI. The study was approved by the ethics committee of our university (approval number: 857). Written, informed consent was obtained from all the participants.

2.2. Pulmonary function testing

A CHSTAC-8900 spirometer (Chest M1 Corp, Tokyo, Japan) was used for PFT, based on the guidelines of the American Thoracic Society and European Respiratory Society [28]. Total lung volume (LV) was determined by the helium dilution method, while the diffusing capacities for carbon monoxide (DL_{co}) and alveolar ventilation were assessed by the single-breath method. Forced vital capacity (FVC) and forced expiratory volume in 1 s (FEV_1) were measured, and their predicted values calculated according to the guidelines of the Japanese Respiratory Society [29].

2.2.1. MRI

A 1.5-T Ingenia CX/Achieva dStream Release 5 MR system (Philips Medical Systems, Amsterdam, The Netherlands) with the patient breathing normally was used for all the MRI studies. A balanced fast-field echo sequence was used in these studies (repetition time 1.84 ms, echo time 0.71 ms, and flip angle 45°). The field of view (FOV) was 384 mm and the matrix size was 192 × 192. The image slice thickness was 13.5 mm with an acquisition time of 121 ms per image. Coronal images were obtained during normal breathing. Sagittal images of the right lung and diaphragm were also obtained during normal breathing.

2.3. Semi-automated lung segmentation method

Sato H et al. demonstrated that cine MRI and several image processing algorithms of MATLAB® R2021b (The MathWorks, Inc, Natick, USA) can be used to perform semi-automatic extraction of the lung [30]. As shown in Fig. 1, the steps used in this process were as follows.

Firstly, the maximum inspiratory image was selected from the time-sequential images and the lung area segmented manually by a single observer for use as a mask image (Fig. 1 **(a)**). Secondly, both the mask and cine images were added to create a weighted cine image (Fig. 1 **(b)**) and the lung area then segmented using the K-means clustering technique (Fig. 1 **(c,d)**). The number of clusters was set as eight in accordance with the K-means.

On the other hand, a manual pulmonary arteriovenous trace (Fig. 1 **(e)**) and making a mask image was performed, and the segmented image and pulmonary arteriovenous mask image then added (Fig. 1 **(f)**).

Finally, the lungs were detected as a contiguous image region with similar signal values using the flood-fill technique (Fig. 1 **(g)**). The processing time with our method was 1 sec/slice.

In the proposed method, the lung area was first extracted manually using one of the maximum inspiratory images. The lung area trace and the pulmonary arteriovenous trace were extracted and used as the mask images. After this task was completed, the following process was automatic: the thorax was segmented using the k-means method, and the pixels with the continuity were extracted. Then, lung extraction was performed automatically for continuous images.

Assuming that no lung area existed outside the lung contour mask image at any time phase, additional processing was performed to increase the signal value outside the lung fields. Because the signal strengths of the lung area and the pulmonary arteriovenous were different, the signals of the pulmonary arteries and veins were lost during segmentation using the k-means method. Then, the pulmonary arteriovenous mask image was used to compensate for the lack of pulmonary arteriovenous area.

2.3.1. MRI measurements of the lung area ratio and lung area change ratio

MRI coronal images of the aortic valve level were selected to measure the lung area. Sequential images of the most stable and frequent respiratory phases from the maximum inspiratory phase to the next inspiratory phase were obtained. The right and left lung areas of each image were marked semi-automatically (Fig. 2a and b). The areas of the

Fig. 1. Algorithm of the semi-automated lung segmentation program.

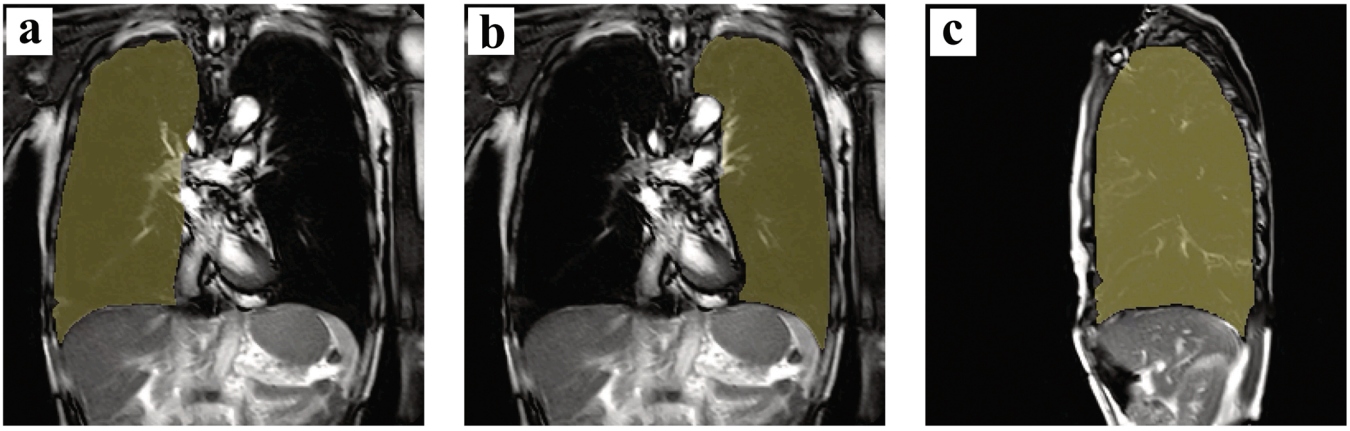

Fig. 2. Images of respiratory dynamics detected by the combination of MATLAB® and cine MRI in a COPD patient. Video images of the respiratory motion are available in Supplementary Figure 1. a, Right coronal section. b, Left lung coronal section.
c, Right lung sagittal section Abbreviations: COPD, chronic obstructive pulmonary disease; MRI, magnetic resonance imaging.

lung segmented on each image were calculated automatically by the program. The values of the measured right and left areas within the markings were added together to obtain the total lung area, with the expiratory lung area/inspiratory lung area calculated to obtain the lung area ratio.

We also measured the times of the inspiratory and expiratory phases. To assess the dynamic changes in the areas of the lung during a respiratory cycle, we measured lung areas in every slice from the start of inspiration until the next inspiratory phase. We used the continuous measurements of lung areas to determine the changes in lung areas (motion speed) per 121 ms interval.

For the manual measurements, the MRI images were also analyzed using ImageJ software (version 1.51j8, available at http://rsb.info.nih.gov/ij/; National Institutes of Health, Bethesda, MD, USA). The evaluations of the Dice index between the program and the manual measurements were calculated.

2.4. Examination of the lung area ratio in the respiratory cycle

The lung area from inspiration to expiration was measured

systematically. Since the time from inhalation to exhalation was different for each patient, the time was normalized. The change in lung area from inhalation to expiration was replotted with an approximate curve, and the area of the middle of the cycle time from inspiratory to expiratory was determined. The middle of the cycle time was determined comprehensively by two respiratory physicians, taking into account time, lung field area during inspiration and expiration, and diaphragmatic displacement. The lung area ratio was calculated from the lung areas at three representative points: inspiration, midpoint, and expiration. The period from inspiration to the midpoint was defined as the "first half," and the period from the midpoint to the exhalation as the "second half.".

2.5. Evaluation of the asynchronous movements of the diaphragm

Evaluation of the asynchronous movements of the diaphragm using a cine image of the sagittal section was also performed. Due to the potential influence of artifacts from the heart and gastrointestinal tract in images of the left lung, the right lung was evaluated in this study. The length of the diaphragm in the anterior-posterior direction in the expiratory image was calculated **(**Fig. 3**a)**. The measured distance was then divided into six equal parts (i.e., seven points). The second point was defined as the “front side point”, the fourth as the “middle point”, and the sixth as the “rear side point” **(**Fig. 3**b-d**).

The midpoint from the apex of the lung to the diaphragm was used as the common y-coordinate.

For each point, the distance from the midpoint of the y coordinate to the diaphragm was then measured using an automatic segmentation image. The signal intensity of the image was binarized as "1" in the lung area and "0" outside of the lung area. The pixels of each of the time phases were counted and the distance measured. The movement of the diaphragm was quantitatively evaluated by plotting the distance on the time axis.

The correlation coefficient of the movement of each of the three points was calculated, followed by comparison of the coefficients between the groups with or without the presence of the asynchronous movements obtained by visual evaluation by two pulmonologists (AS and NK).

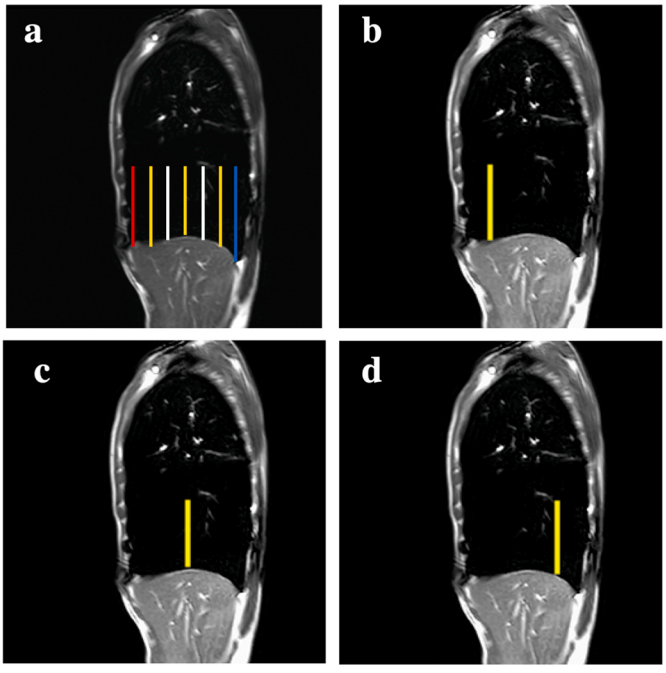

Fig. 3. Measurements of diaphragm movement at three points. **Note:** The measured distance was then divided into six equal parts (i.e., seven points, from the red line to the blue line). The vertical distance at three points of the diaphragm was measured over the respiratory cycle (location 1, front side; location 2, middle point; location 3, rear side). The length of the yellow line changes over time. The movement of the diaphragm was calculated from the length. Video images of the respiratory motion are available in Supplementary Fig. 2a**-c**.

2.6. Statistical analysis

All the statistical analyses were performed using JMP Pro version 13.0 software (SAS Institute, Cary, NC, USA). Differences between the two groups were evaluated by the Student’s *t*- test for parametric data or the Mann-Whitney *U* test for data that did not pass the normality test (Shapiro-Wilk test). The Pearson bivariate correlation coefficient was calculated to evaluate the association between two variables for parametric data, while the Spearman test was used to examine the associations between nonparametric data. P values < 0.05 were considered significant.

To examine the agreement of the calculated lung area in inspiratory and expiratory images between the manual and semi-automatic methods, the Dice index was calculated as follows:

$$\text{Dice index} = 2*|A \cap B| / |A| + |B|$$

A represents the area for manual extraction and B the area for semi-automatic extraction.

3. Results

3.1. Detection of motion of lung areas and the diaphragm

Examples of detected lung area using cine MRI and the semi-automated software are shown in Fig. 2**a** and **b.** Videos are shown in Supplementary Figs. 1a and 1b. The right and left lungs were detected separately.

Supplementary material related to this article can be found online at doi:10.1016/j.ejro.2022.100442.

Examples of diaphragmatic motion on sagittal images are also shown in Fig. 2**c.** Videos are shown in Supplementary Fig. 1c. The sagittal images of the right lung showed the bizarre motion of the diaphragm more clearly.

Supplementary material related to this article can be found online at doi:10.1016/j.ejro.2022.100442.

3.2. Results of the Dice index

The Dice index between the semiautomated method and the manual

method was excellent (Dice index = 0.97 ± 0.03). The area of lung extraction was similar between the manual and semi-automatic measurements. The average measurement time with the manual method was 20.7 ± 6.7 min for each image series.

3.3. Characteristics of the study participants

The demographics of the 10 normal participants and 21 COPD patients are shown in Table 1. These demographics have been described previously [17]. Compared to the normal volunteers, the COPD patients were significantly older, had significantly lower FEV_1, and a higher residual volume per total lung capacity (RV/TLC). The majority of COPD patients were classified as GOLD stage III to IV (severe to very-severe) disease. All the COPD patients underwent bronchodilator therapy (long-acting muscarinic antagonists (LAMA), n = 1, LAMA+ long-acting β-2 agonizts (LABA), n = 5, LAMA+ inhaled corticosteroids (ICS), n = 1, LABA+ICS, n = 1, LAMA+LABA+ICS, n = 13).

3.4. Change in lung area during free breathing

The lung area ratio in the first half was significantly higher in both normal subjects and COPD patients **(**Fig. 4**).** In the COPD patients, the change in the lung area ratio from the first half to the second half was significantly lower compared to that observed in the normal subjects.

(COPD 0.962±0·02, vs Normal 0.932±0·02, p = 0.006)·

3.5. The correlation between lung area ratio and physiological parameters

As shown in Table 2, the lung area ratio in the first half of the respiratory cycle showed a significant inverse correlation with FEV_1%pred, FEV_1/FVC, and a significant positive correlation with RV%pred ($r = -0.54$, $p = 0.01$, $r = -0.50$, $p = 0.01$, and $r = 0.50$, $p = 0.03$, respectively).

Supplementary Table 1 shows the correlation between PFTs and the lung area ratio in the second half of the respiratory cycle, while Supplementary Table 2 shows the correlation between PFTs and the lung area ratio (expiration/inspiration).

Table 1
Demographic data of the 31 study subjects.

	Normal (n = 10)	COPD (n = 21)	*P*-value
Age (yr)	31.9 ± 1.5	68.1 ± 9.1	< 0.0001
Male sex (%)	100	90.4	
BMI (kg/m^2)	21.5 ± 1.2	19.6 ± 3.0	0.076
GOLD classification (I/II/III/IV)		0 (0%) / 1 (4.8%) / 6 (28.6%) / 14 (66.7%)	
Pulmonary function test			
FVC %predicted (%)	102.2 ± 14.5	75.4 ± 22.4	0.003
FEV_1 (L)	4.23 ± 0.4	0.89 ± 0.3	< 0.0001
FEV_1%predicted (%)	99.9 ± 11.5	32.8 ± 11.2	< 0.0001
FEV_1/FVC (%)	87.0 ± 6.3	35.3 ± 7.0	< 0.0001
FRC %predicted (%)	120.9 ± 15.2	126.1 ± 26.6	0.59
RV %predicted (%)	123.9 ± 38.0	150.2 ± 38.2	0.098
RV/TLC (%)	27.9 ± 7.8	51.8 ± 9.0	< 0.0001
DLco/VA %predicted (%)	114.9 ± 11.4	51.9 ± 22.1	< 0.0001

Note: Data are expressed as mean ± standard deviation.
Abbreviations: COPD, chronic obstructive pulmonary disease; BMI, body mass index; GOLD, COPD assessment test; FVC, forced vital capacity; $FEV_{1.0}$, forced expiratory volume in 1 s; FRC, functional residual capacity; RV, residual volume; TLC, total lung capacity; DLco/VA, diffusing capacity for carbon monoxide per liter of lung volume; LV, lung volume.

3.6. Asynchrony of the diaphragmatic movements

A sagittal image was used to evaluate the distance of the diaphragm movement and asynchronous motion of the diaphragm **(**Fig. 3**a-d).** Videos are shown in Supplementary Fig. 2a-2d. The distance of the diaphragm at each point was not significantly different between the two groups **(**Fig. 5**a-c).** Interestingly, the correlation coefficients of the synchrony at each point (location 1 vs. location 2, location 1 vs. location 3, location 2 vs. location 3) in the COPD group were significantly lower than those in the control group ($p = 0.005$, $p = 0.001$, $p = 0.022$, respectively (Fig. 5**d-f**).

Supplementary material related to this article can be found online at doi:10.1016/j.ejro.2022.100442.

The correlation coefficient for each point in the group with visible see-saw like movements of the diaphragm (n = 13) was significantly lower than those in the group without see-saw like movements of the diaphragm (n = 18) (value = −0.36 vs 0.95, p = 0.001) **(**Fig. 6**).**

4. Discussion

The main findings of the present study were as follows: 1) We combined cine MRI and several image processing algorithms of a programming language to perform semi-automatic extraction of the lungs. This allowed us to extract the lung area with the same accuracy as manual extraction. 2) In the process from inhalation to expiration, the rate of area change in the first half was larger than that observed in the second half. This indicated that the rate of change in the lung field due to free-breathing was not constant. In addition, the rate of change of lung area was significantly lower in COPD patients than that measured in the normal controls. 3) In the sagittal plane using Cine MRI, the same lung field extraction method was performed to evaluate diaphragmatic motion. The presence of an asynchronous diaphragmatic motion was evaluated quantitatively in the COPD patients.

In the current study, we used a semi-automatic program to extract the lung fields from Cine MRI [31]. This showed that the program extracted the lung field region with the same level of accuracy as achieved by the conventional manual extraction.

For segmentation of lungs using thoracic cine MRI, automatic and semi-automatic extraction methods using 3D region growing [32], a combination of confidence-connectedness and fuzzy-connectedness algorithms [33], and an atlas-based estimation [34] have been reported. On the other hand, there are no reports on lung field segmentation using cine MRI and the k-means method. Conventionally, MRI images of the head [35,36] and mammary gland [37] have been segmented using the k-means method. The k-means method is now used for segmenting MRI images because the number of clusters is usually determined according to each region in the human body [38]. For example, the head region is assigned to four groups: white matter (WM), grey matter (GM), cerebrospinal fluid (CSF), and tumor lesions, while the mammary gland is also divided into three or four clusters.

Determination of the number of clusters is essential when adapting to a chest MRI. Compared to other organs, the chest region has more complicated structures with various signal intensities on the image. In addition, the k-means method is an unsupervised algorithm that assigns each voxel to a cluster (e.g., adipose tissue) based on its grey-scale intensity and distribution. In the presence of image signal inhomogeneity or artifacts, the method may not perform correct segmentation as achieved using the other algorithms [39]. We addressed these concerns by first manually extracting the lung fields of the inspiratory image, which we determined to be the mask image. By adding this mask image to the cine image, we could stably segment the cine image by setting the number of clusters to eight because of the difference in signal intensity between the cine image and the lung fields.

We propose that the imaging sequence is also essential for lung field segmentation in the chest MRI. There are numerous reports of imaging using the 3D GRE (FLASH) [32] and UTE [40] methods. These methods

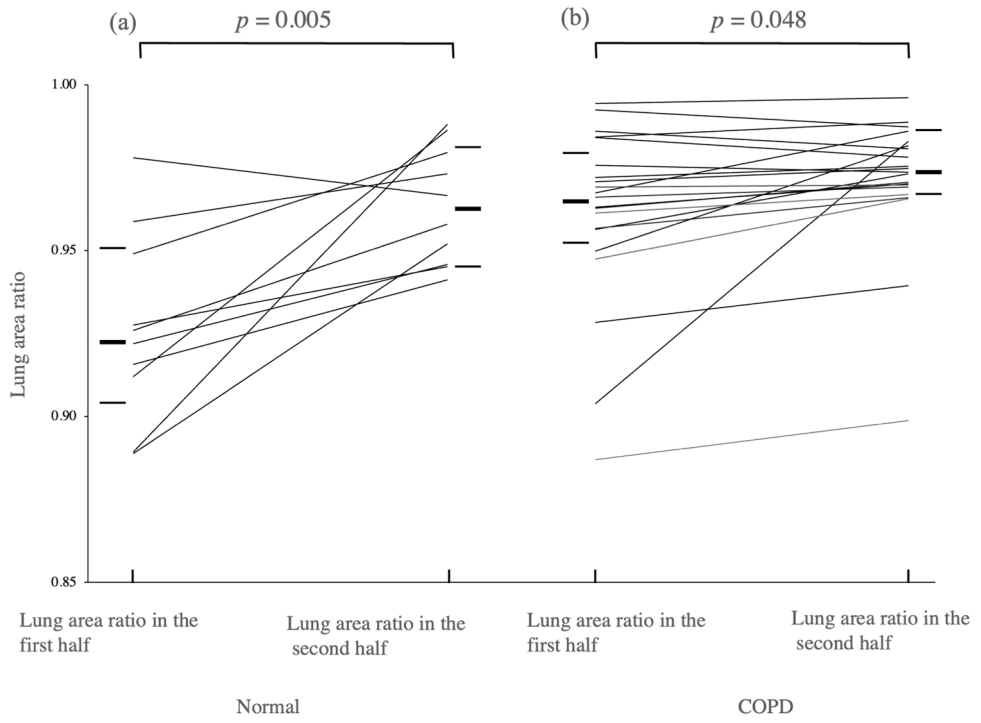

Fig. 4. Comparisons of the rate of change between from the inspiration peak to the midpoint and from the midpoint to the expiration peak. **Note:** The change in rate was compared between the inspiration peak to the midpoint and from the midpoint to the expiration peak using the Wilcoxon signed-rank test. The thick horizontal bars at the sides of each graph show the median, while the thin horizontal bars at the sides of each graph show the interquartile range.

Table 2
Correlation between the MRI lung area ratio (at the point of the first half of the respiratory cycle) and physiological parameters in COPD patients.

	Correlation coefficient	
Pulmonary function test	r	*P*-value
FEV_1 (L)	-0.31	NS
FEV_1%predicted (%)	-0.54	0.01
FEV_1/FVC (%)	-0.50	0.01
FRC %predicted (%)	0.23	NS
RV %predicted (%)	0.50	0.03
RV/TLC	0.37	NS

Note: Data are expressed as mean ± standard deviation.
Abbreviations: COPD, chronic obstructive pulmonary disease; FEV_1, forced expiratory volume in 1 s; FRC, functional residual capacity; RV, residual volume; TLC, total lung capacity, NS, not significant.

have excellent spatial resolutions. On the other hand, the SSFP method has an excellent temporal resolution [41]. In the current study, we used the SSFP method to image cine MRI. The SSFP method is a sequence susceptible to magnetic changes, with artifacts often appearing at the boundaries of the lung fields and the four corners of the image. Our method reduced the effect of magnetic susceptibility by increasing the signal intensity in the periphery of the lung field, which allowed us to perform accurate segmentation.

The lung area change rate in the first and second half of expiration was predominantly greater in the first half. During the expiratory cycle, the change in lung area did not vary at a constant rate but was more prominent in the first half and more gradual in the second half. These results were seen in both normal subjects and the COPD patients. In a recent report using dynamic chest radiography under forced breathing, the diaphragmatic changes during expiration were not constant [42]. The present study showed that the change in lung field area under free-breathing was also not constant. The magnitude of the rate of change itself was significantly smaller in the COPD patients. Regarding the relationship with disease severity, the correlation between the area change in the first half and pulmonary function was significant compared to the lung area ratio obtained from the second half. Evaluating the change at the first half of exhalation could add essential information about respiratory dynamics to the conventional method, such as evaluating the change in the area between the two points of inspiration and expiration.

The same program was used to evaluate asynchronous movements from cine images of sagittal sections. The distance of the diaphragm at each point was not significantly different between the two groups. However, interestingly there was a decrease in the simultaneity of the diaphragm at each point in the COPD group. Iwasawa et al. evaluated the change in lung area and the flatness of the diaphragm using inspiratory and expiratory MRI images in order to assess asynchronous movements in patients with COPD [16]. In the current study, we quantitatively evaluated the simultaneity of motions at multiple points of the diaphragm and showed that the correlation coefficients were significantly decreased in cases with visual evidence of asynchronous movements. In order to diagnose the presence of asynchronous movements it might be helpful to carry out quantitative assessment to evaluate the asynchrony of bizarre movements. This indicates that it is difficult to make similar evaluations with other modalities.

The present study proposed a semi-automated lung field extraction method and performed continuous lung area extraction and quantitative evaluation. The assessment will be useful for evaluating the pathophysiology of COPD and determining the effects of personalized treatment, comprehensive respiratory rehabilitation and surgical interventions in the near future [43].

4.1. Limitations

This study had several limitations. First, the semi-automatic extraction was a verification of only SSFP sequence images, and it is necessary to examine whether other sequences can be applied to dynamic analysis. Second, only the right side of the sagittal section was analyzed. The left side was not analyzed because of the potential influence of artifacts

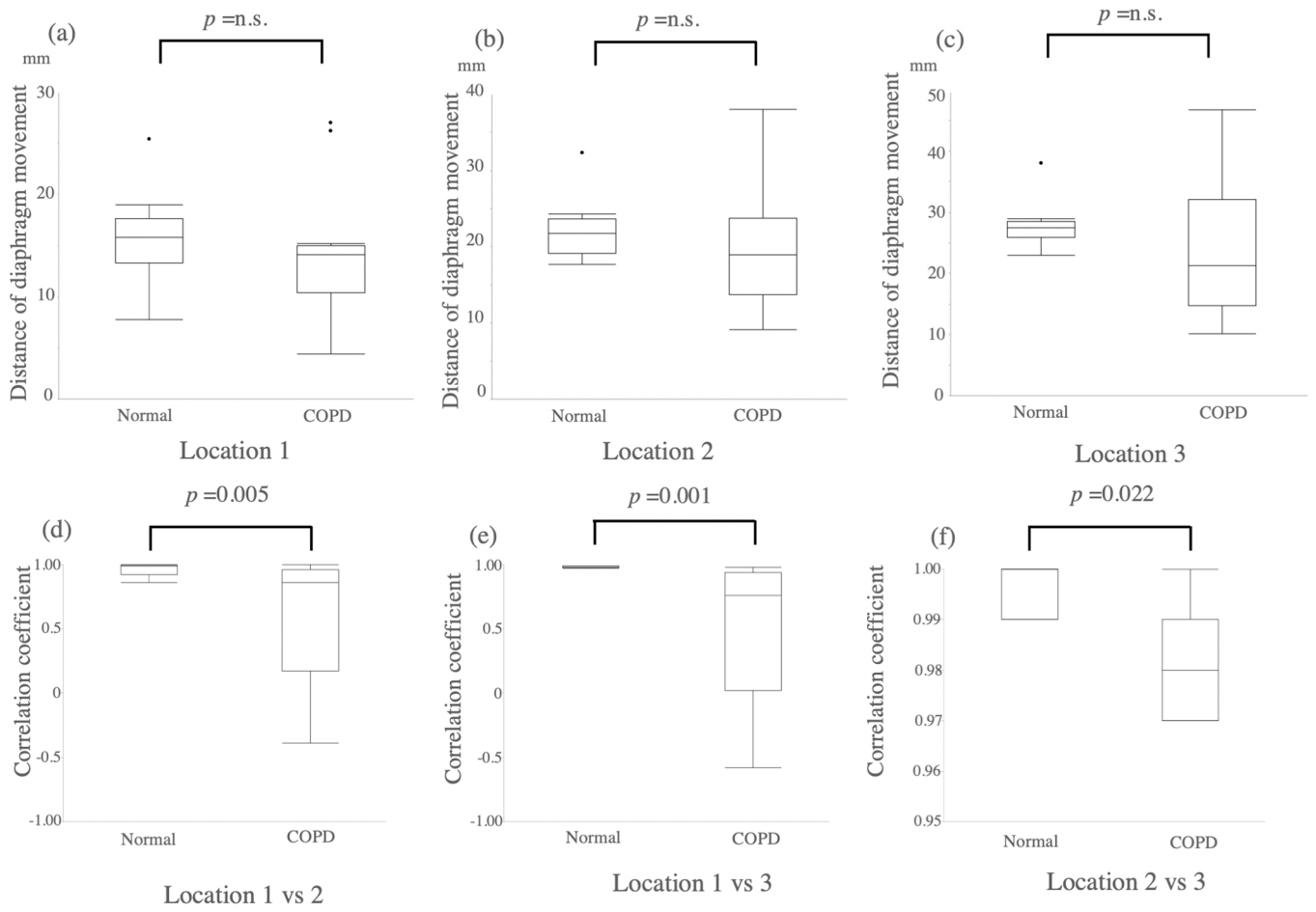

Fig. 5. Comparisons of the distance of the diaphragm and asynchrony of the diaphragm between the normal subjects and patients with COPD. Note: Upper row: Comparisons of the distance of the diaphragm at each point. Lower row: Comparisons of the simultaneity of diaphragmatic movements at each point. The values show the correlation coefficient. 1 represents a positive correlation, 0 the least correlated, and − 1 a negative correlation.

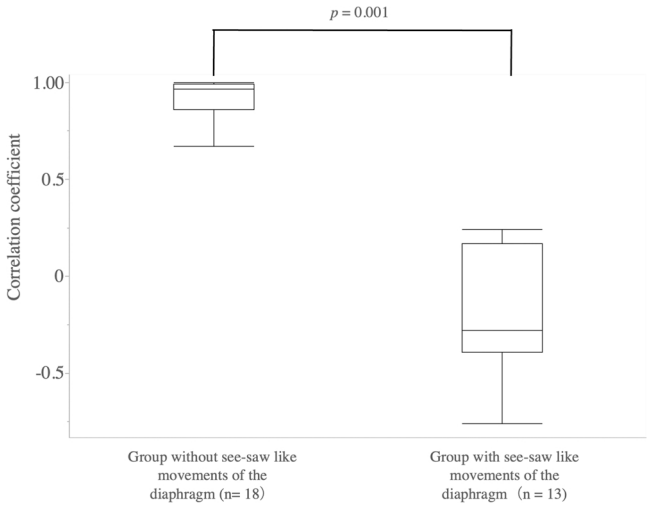

Fig. 6. Comparisons of asynchrony of the diaphragm between patients with and without see-saw like movements of the diaphragm. Note: The positions were measured at the front and rear sides. The value shows the correlation coefficient. 1 represents a positive correlation, 0 the least correlated, and − 1 a negative correlation.

associated with cardiac motion and banding from the gastrointestinal tract, and should therefore be examined in future studies. Third, regarding the correlation with respiratory function, our data was obtained from a small number of participants recruited from a single institution. Most patients had severe to very severe COPD. Therefore, these preliminary results should be confirmed in a larger patient cohort covering all stages of age-matched COPD.

5. Conclusion

Semi-automated extraction of lung area from Cine MRI allowed quantitative assessment of changes in lung area and asynchrony of the diaphragm over the respiratory cycle. Parameters using cine MRI can provide essential information that reflects respiratory kinetics in COPD patients.

Funding Statement

This research was partially supported by the Ministry of Education, Science, Sports and Culture, Grant-in-Aid for Scientific Research (C) (19K12816), and the Chiba Foundation for Health Promotion & Disease Prevention (No.1272). The funders had no role in study design, data collection and analysis, decision to publish, or preparation of the manuscript.

Ethical statement

This study was approved by the ethics committee of Chiba University (approval numbers: 857). Written informed consent was obtained from all the participants.

Author contributions

HS, NK, and AS conceived and designed the paper. AS and NK collected the data. HS, NK and AS analyzed the data. HS NK, YI, CY, YM and HH contributed to the software, materials/analysis tools and validation. HS and NK contributed to the writing of the manuscript. HS, NK, KT and TS contributed to the review and editing. All authors read and approved the final manuscript.

Appendix A. Supporting information

Supplementary data associated with this article can be found in the online version at doi:10.1016/j.ejro.2022.100442.

References

[1] J.C. Hogg, P.D. Paré, T.L. Hackett, The contribution of small airway obstruction to the pathogenesis of chronic obstructive pulmonary disease, Physiol. Rev. 97 (2) (2017) 529–552.
[2] WHO. The top 10 causes of death. Geneva: World Health Organization, 2020.
[3] Global Initiative for Chronic Obstructive Lung Disease. 2020 Global strategy for prevention, diagnosis and management of COPD. Available at: ⟨https://goldcopd.org/wp-content/uploads/2021/11/GOLD-POCKET-GUIDE-2022-v1.1–22Nov2021_WMV.pdf⟩, (accessed 1 November 2021).
[4] S. Matsuoka, G.R. Washko, T. Yamashiro, et al., National Emphysema Treatment Trial Research Group. Pulmonary hypertension and computed tomography measurement of small pulmonary vessels in severe emphysema, Am. J. Respir. Crit. Care Med. 181 (3) (2010) 218–225.
[5] P.R. Goddard, E.M. Nicholson, G. Laszlo, et al., Computed tomography in pulmonary emphysema, Clin. Radiol. 33 (4) (1982) 379–387.
[6] G. Camiciottoli, M. Bartolucci, N.M. Maluccio, et al., Spirometrically gated high-resolution CT findings in COPD: lung attenuation vs lung function and dyspnea severity, Chest 129 (3) (2006) 558–564.
[7] M. Hasegawa, Y. Nasuhara, Y. Onodera, et al., Airflow limitation and airway dimensions in chronic obstructive pulmonary disease, Am. J. Respir. Crit. Care Med. 173 (12) (2006) 1309–1315.
[8] E. Ogawa, Y. Nakano, T. Ohara, et al., Body mass index in male patients with COPD: correlation with low attenuation areas on CT, Thorax 64 (1) (2009) 20–25.
[9] Tanabe N., Muro S., Hirai T., et al. Impact of exacerbations on emphysema progression in chronic obstructive pulmonary disease. Am J Respir Crit Care Med 201;183(12):1653–1659.
[10] R.G. Barr, S. Mesia-Vela, J.H. Austin, et al., Impaired flow-mediated dilation is associated with low pulmonary function and emphysema in ex-smokers: the Emphysema and Cancer Action Project (EMCAP) Study, Am. J. Respir. Crit. Care Med 176 (12) (2007) 1200–1207.
[11] F. Laghi, M.J. Tobin, Disorders of the respiratory muscles, Am. J. Respir. Crit. Care Med. 168 (1) (2003) 10–48.
[12] T. Iwasawa, S. Kagei, T. Gotoh, et al., Magnetic resonance analysis of abnormal diaphragmatic motion in patients with emphysema, Eur. Respir. J. 19 (2) (2002) 225–231.
[13] R. Tanaka, Dynamic chest radiography: flat-panel detector (FPD) based functional X-ray imaging, Radio. Phys. Technol. 9 (2) (2016) 139–153.
[14] E. Mochizuki, Y. Kawai, K. Morikawa, et al., Difference in local lung movement during tidal breathing between COPD patients and asthma patients assessed by four-dimensional dynamic-ventilation CT scan, Int. J. Chron. Obstruct Pulmon Dis. 15 (2020) 3013–3023.
[15] Tanaka Y., Ohno Y., Hanamatsu S., et al. State-of-the-art MR Imaging for Thoracic Diseases. Magn Reson Med Sci. 2021 Apr 29.
[16] Iwasawa T., Takahashi H., Ogura T., et al. Influence of the distribution of emphysema on diaphragmatic motion in patients with chronic obstructive pulmonary disease. Jpn J Radiol 201;29(4):256–264.
[17] A. Shimada, N. Kawata, H. Sato, et al., Dynamic quantitative magnetic resonance imaging assessment of areas of the lung during free-breathing of patients with chronic obstructive pulmonary disease, Acad. Radiol. S1076–6332 (21) (2021), 00205-1.
[18] C. Plathow, M. Schoebinger, F. Herth, et al., Estimation of pulmonary motion in healthy subjects and patients with intrathoracic tumors using 3D-dynamic MRI: initial results, Korean J. Radiol. 10 (6) (2009) 559–567.
[19] Y. Yang, E. Van Reeth, C.L. Poh, et al., A spatiotemporal-based scheme for efficient registration-based segmentation of thoracic 4-D MRI, IEEE J. Biomed. Health Inf. 18 (3) (2014) 969–977.
[20] W.C. Chu, A.M. Li, B.K. Ng, et al., Dynamic magnetic resonance imaging in assessing lung volumes, chest wall, and diaphragm motions in adolescent idiopathic scoliosis versus normal controls, Spine 31 (19) (2006) 2243–2249.
[21] H. Hatabu, Y. Ohno, W.B. Gefter, et al., Expanding applications of pulmonary MRI in the clinical evaluation of lung disorders: Fleischner society position paper, Radiology 297 (2) (2020) 286–301.
[22] R.S. Tavares, J.M. Chirinos, L.I. Abe, et al., Temporal segmentation of lung region from MRI sequences using multiple active contours, Annu. Int. Conf. IEEE Eng. Med. Biol. Soc. 2011 (2011) 7985–7988.
[23] R. Tetzlaff, T. Schwarz, H.U. Kauczor, et al., Lung function measurement of single lungs by lung area segmentation on 2D dynamic MRI, Acad. Radiol. 17 (4) (2010) 496–503.
[24] T. Böttger, K. Grunewald, M. Schöbinger, et al., Implementation and evaluation of a new workflow for registration and segmentation of pulmonary MRI data for regional lung perfusion assessment, Phys. Med. Biol. 52 (5) (2007) 1261–1275.
[25] T. Böttger, T. Kunert, H.P. Meinzer, et al., Application of a new segmentation tool based on interactive simplex meshes to cardiac images and pulmonary MRI data, Acad. Radiol. 14 (3) (2007) 319–329.
[26] M. Schiwek, S.M.F. Triphan, J. Biederer, et al., COSYCONET study group. Quantification of pulmonary perfusion abnormalities using DCE-MRI in COPD: comparison with quantitative CT and pulmonary function, Eur. Radiol. 32 (3) (2022) 1879–1890.
[27] P.W. Jones, G. Harding, P. Berry, et al., Development and first validation of the COPD Assessment Test, Eur. Respir. J. 34 (3) (2009) 648–654.
[28] M.R. Miller, J. Hankinson, V. Brusasco, et al., Standardisation of spirometry, Eur. Respir. J. 26 (2) (2005) 319–338.
[29] Committee of Pulmonary Physiology in Japanese Respiratory Society. Guidelines for pulmonary function tests: spirometry, flow-volume curve, diffusion capacity of the lung. 1st ed.: Nihon Kokyuki Gakkai Zasshi; 2004; 1–56.
[30] H. Sato, N. Kawata, A. Shimada, et al., [Semi-automated Segmentation of Lungs Using the k-means Method in Cine MRI], Nihon Hoshasen Gijutsu Gakkai Zasshi 77 (11) (2021) 1298–1308.
[31] N. Ohkura, K. Kasahara, S. Watanabe, et al., Dynamic-ventilatory digital radiography in air flow limitation: a change in lung area reflects air trapping, Respiration 99 (5) (2020) 382–388.
[32] P. Kohlmann, J. Strehlow, B. Jobst, et al., Automatic lung segmentation method for MRI-based lung perfusion studies of patients with chronic obstructive pulmonary disease, Int. J. Comput. Assist Radiol. Surg. 10 (4) (2015) 403–417.
[33] J. Tokuda, M. Schmitt, Y. Sun, et al., Lung motion and volume measurement by dynamic 3D MRI using a 128-channel receiver coil, Acad. Radiol. 16 (2009) 22–27.
[34] N.J. Tustison, K. Qing, C. Wang, et al., Atlas-based estimation of lung and lobar anatomy in proton MRI, Magn. Reson. Med. 76 (2016) 315–320.
[35] J. Qiao, X. Cai, Q. Xiao, et al., Data on MRI brain lesion segmentation using K-means and Gaussian Mixture Model-Expectation Maximization, Data Brief. 27 (2019), 104628.
[36] M. Nasor, W. Obaid, Detection and localization of early-stage multiple brain tumors using a hybrid technique of patch-based processing, k-means clustering and object counting, Int. J. Biomed. Imaging 2020 (2020), 9035096, 9 pages.
[37] A. Niukkanen, O. Arponen, A. Nykanen, et al., Quantitative volumetric k-means cluster segmentation of fibroglandular tissue and skin in breast MRI, J. Digit Imaging 31 (2018) 425–434.
[38] Wu M.N., Lin C.C., Chang C.C. Brain Tumor Detection Using Color-Based K-Means Clustering Segmentation. Third International Conference on Intelligent Information Hiding and Multimedia Signal Processing (IIH-MSP 2007), 2007, 245–250.
[39] W.F. Sensakovic, S.G. Armato 3rd, A. Starkey, et al., Automated lung segmentation of diseased and artifact-corrupted magnetic resonance sections, Med. Phys. 33 (9) (2006) 3085–3093.
[40] W. Zha, S.B. Fain, M.L. Schiebler, et al., Deep convolutional neural networks with multiplane consensus labeling for lung function quantification using UTE proton MRI, J. Magn. Reson Imaging 50 (4) (2019) 1169–1181.
[41] O. Bieri, K. Scheffler, Fundamentals of balanced steady state free precession MRI, J. Magn. Reson Imaging 38 (1) (2013) 2–11.
[42] T. Hida, Y. Yamada, M. Ueyama, et al., Decreased and slower diaphragmatic motion during forced breathing in severe COPD patients: time-resolved quantitative analysis using dynamic chest radiography with a flat panel detector system, Eur. J. Radiol. 112 (2019) 28–36.
[43] K. Martini, C. Caviezel, D. Schneiter, G. Milanese, I. Opitz, W. Weder, T. Frauenfelder, Dynamic magnetic resonance imaging as an outcome predictor for lung-volume reduction surgery in patients with severe emphysema, Eur. J. Cardiothorac. Surg. 55 (3) (2019) 446–454.